Diamond-reinforced cutting tools using laser-based additive manufacturing

Kellen D. Traxel and Amit Bandyopadhyay*
W. M. Keck Biomedical Materials Research Laboratory
School of Mechanical and Materials Engineering
Washington State University, Pullman, WA 99164, USA
E-mail: amitband@wsu.edu

Abstract

Production-volume and cost requirements currently limit machine tool manufacturers' ability to produce application-specific tooling with traditional methods, motivating the development of innovative manufacturing technologies. To this end, we detail a manufacturing framework for the design and production of application-specific cutting tools based on industry standard tungsten carbide-cobalt (WC-Co)-based "carbide" cutting materials using additive manufacturing (AM). Herein, novel diamond-reinforced carbide structures were designed and manufactured via AM and subsequently tested in comparison to current commercial products that are traditionally-processed. The resulting diamond-reinforced composites were free from large scale cracking and maintained microstructures with multiple reinforcing phases. Diamond incorporation had a remarkable effect on the processing, microstructure, and machining performance of the WC-Co based material in comparison to a commercial carbide cutting tool of similar composition as well as the base WC-Co matrix. Detailed microstructure and phase analysis, as well as machining experiments, demonstrate the ability to exploit laser-based directed energy deposition (DED)-based AM to create multifunctional cutting tools that can be designed to meet ever-increasing manufacturing demands across many industries.

Keywords: Additive manufacturing; cutting-tool materials; tungsten carbide; diamond reinforcement; directed-energy-deposition.

1.0 Introduction

Machine-tool manufacturers supply the equipment necessary to fabricate parts that turn into biomedical implants, engine components, pressure vessels, and numerous other critical components across many industries. The machining industry alone is projected to exceed $415 billion by the year 2022, owing to the growing demand of customers to work on highly application-specific jobs with exotic materials, and with decreased lead times to the end-user [1]. These demands put strain on manufacturers to innovate many design aspects that affect tool cost and performance such as cutting-tip geometry, base material, multi-layer coating, and indexability, among many others, and have motivated recent investigations in our fundamental understanding of machining processes and emerging manufacturing technologies [2–4]. Historically, success has been achieved via improving a single design factor in regards to a specific, singular application for a particular workpiece material or desired final part surface finish or geometry [5,6]. However, with complex design concepts as well as the onset of hybrid additive manufacturing (AM) techniques as evidenced in the work of Gomez et al. [7], more components are relying on innovative methods of tool fabrication that offer manufacturers the ability to combine improvements and rapidly iterate to find the best design while decreasing overall cost and processing complexity.

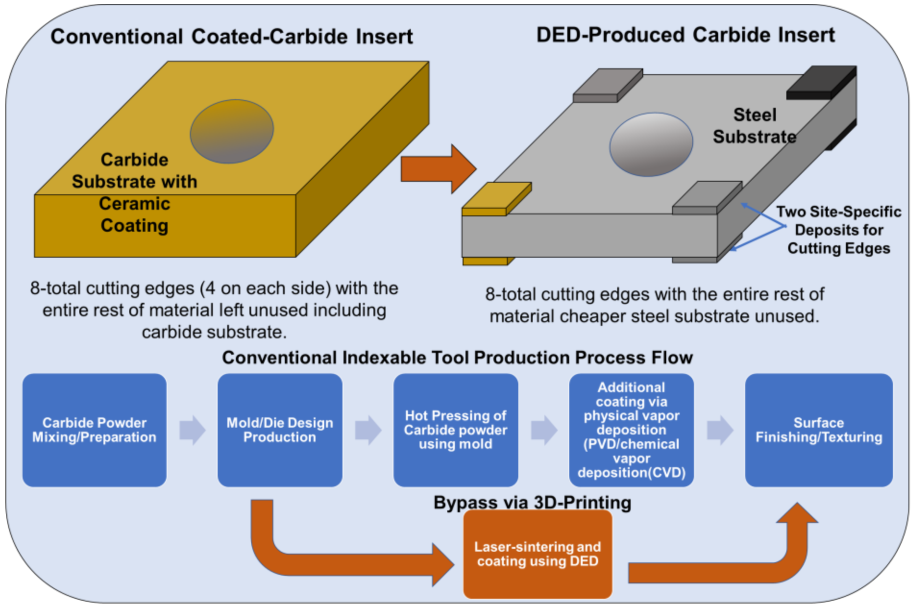

Figure 1: Comparison of tool production using traditional processing via directed energy deposition based additive manufacturing.

Most traditional tool manufacturing workflows are optimized for high-volume production, meaning that meeting the needs for one-off parts in challenging applications is difficult to achieve economically. The most advanced tools are composite-based cemented carbides that combine high-temperature strength, abrasion resistance and ductility, and are comprised primarily of a metal binder (typically 4 to 20 weight%) and a reinforcing ceramic phase (typically 80 to 96 weight%) with additional coatings of varying compositions and thickness depending on the workpiece material, desired final geometry, surface finish, etc. [8]. To achieve this, traditional processing methods such as hot pressing/sintering and ceramic coating via physical vapor deposition (PVD) or chemical vapor deposition (CVD) are utilized in different set-ups, and typically limited to a single configuration of tool material and coating combination, meaning that each tool is fabricated with a single application in mind and must be produced in large quantity to decrease the overall manufacturing cost (see **Fig. 1**). Laser-based AM, primarily directed-energy-deposition (DED), is an emerging technology that shows promise for low-volume, specialized applications, making it relevant although largely unexplored in the cutting tools industry [9]. DED is a powder-flow AM process that enables multiple materials to be laser-melted and deposited on a substrate simultaneously, or in succession, to manufacture net-shape metallic structures [10–12], functionally-graded structures [13,14], die-tooling [15,16], and ceramic-based composites [17,18], indicating the propensity for it to be applied towards manufacturing multi-functional tool materials relevant to cutting applications. In addition, the multi-material nature of this process (**Figs. 1 & 2**), enables manufacturers to rapidly experiment

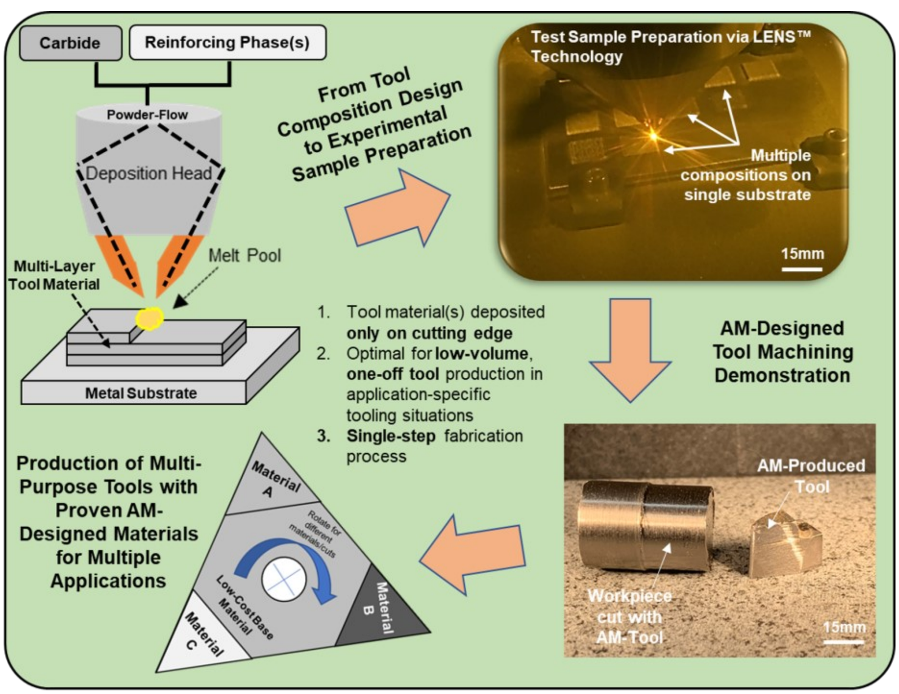

Figure 2: Framework for rapid tool development via laser-based additive manufacturing which leverages the ability to design compositions on the fly and create multi-application tools with site-specific materials.

with different tool material chemistries and coating schemes to iterate on previous designs, or to understand the effect of different reinforcement on cutting performance.

A novel multifunctional tool workflow concept enabled via DED-based processing is shown in **Fig. 2**, whereby, multiple designed compositions are fabricated on a single substrate to enable cutting of multiple workpiece materials and/or cutting applications with a single bulk tool, without the need for multiple cutting setup procedures. Different materials can be tested and iterated rapidly, with the highest performing material utilized in various insert designs that can be used in different cutting applications. To the best of the authors' knowledge, this design does not currently exist in the market, and while previously proposed [19] using Stellite™ as a base tool material, has yet to be fully realized in the literature in terms of a full-scale tool development platform with multiple compositions rapidly tested to fit the needs of different cutting applications. While several authors have shown the ability to process WC-Co (cemented carbide)-based materials additively using powder-bed fusion processes [20–22], DED is the only AM method capable of achieving this insert concept due to the ease of changing feedstock material. In addition, there is still a fundamental gap in our understanding of how additively manufactured tools behave in comparison to commercial, traditionally-produced products, specifically in regards to defects and porosity that can occur during printing and potentially lead to premature failure [23,24]. If possible, to fabricate and demonstrate DED-processed tools in cutting applications, this process would provide a unique set of advantages to tool manufacturers and end users than what is currently available.

To demonstrate the ability to fabricate the tool concept outlined in **Fig. 2**, we have chosen to explore the variable reinforcement of WC-Co "cemented carbide" with synthetic diamond (henceforth "diamond dust", or DD) for enhanced cutting performance in a soft aluminum workpiece as well as harder, more difficult-to-machine, titanium material. WC-Co is one of the main carbide composites used in the cutting tool industry. While it serves most applications well owing to its toughness (from cobalt) and wear resistance (from WC and other secondary phases), most cutting tools require multi-layer hard ceramic coatings, or reinforcement to increase the tool longevity and overall cutting performance for different applications. As stated previously, these coating methods are multi-step processes, and it is envisioned that DED-based technology can combine a super-hard reinforcing material such as synthetic diamond during processing to further enhance the cutting performance of the carbide material. We hypothesize that novel diamond-reinforced carbide tool materials can be processed via DED and exhibit improved cutting performance in comparison to the base carbide coating as well as commercial products, in different cutting applications. Several previous works have shown that diamond can be processed as a reinforcing phase in both copper and nickel-based alloys using powder-bed-fusion methods [25,26]. Additionally, diamond has been processed successfully using several powder-based sintering methods [27,28]. To this end, two separate reinforcing samples incorporating 2.5wt% DD and 5wt% DD into a WC-Co matrix, were fabricated for microscopy and tool grinding/testing. A control composition of WC-Co was processed, and a secondary control of a similar uncoated WC-Co composition (but traditionally-processed) cutting tool based on VNMG-332 insert geometry was utilized in the cutting tests for comparison of tool performance in different cutting applications. Scanning electron microscopy (SEM), Energy Dispersive Spectroscopy (EDS), and X-Ray Diffraction (XRD) were used to characterize the microstructure and phase evolution of the composites, as well as analyzed the nature of the wear surfaces on each tool after machining aluminum and titanium workpieces via turning. Discussion on how this tooling concept can be expanded upon and utilized by manufacturers in modern machine shops is included at the end of the article.

2.0 Materials and methods

Directed-energy-deposition for application-specific tooling: Our Laser Engineered Net Shaping (LENS™) machine (Optomec LENS™ 750, Albuquerque, NM) operates a continuous-

Table 1: Processing parameters for each composition.

Composition	Laser Power (W)	Hatch Scan Speed (mm/s)	Hatch Spacing (mm)	Final Height (mm)	Layer Thickness (µm)	Hatch Angle Sequence
WC-Co (1st Attempt)	400	6	0.5	0.76 ± 0.16	152 ± 32	Layer 1: 0° Layer 2: 120° Layer 3: 240° Layer 4: 180° Layer 5: 120°
WC-Co (2nd Attempt)	450	6		1.43 ± 0.01	286 ± 2	
WC-Co (Optimized)	475	5		1.38 ± 0.22	276 ± 44	
WC-Co+ 2.5wt%DD	475	5		0.79 ± 0.01	158 ± 3	
WC-Co+ 5wt%DD	475	7.5		0.66 ± 0.01	132 ± 5	

wave 500W Nd:YAG laser which is focused on the top of a build substrate which is bolted to an NC-controlled plate able to move in the x and y directions, with the deposition-head moving in the Z-direction on each layer (shown conceptually in **Fig. 2**). The chamber enclosing the deposition head and build plate is maintained in an argon atmosphere (O_2 ppm<15) to limit oxidation of the built structure. Further discussion of this technique can be found in our previous references [29,30]. Both starting powders, WC-12wt%Co (or WC-Co henceforth) (PAC 125, Powder Alloy Corporation, Loveland, Ohio, USA) and granular synthetic diamond dust (or DD henceforth) (Lands Superabrasives, New York, New York, USA), were pre-sieved to a 50-150µm particle size range, typical for DED systems (see **Fig. 3**). To fabricate the tooling materials, a single powder hopper was loaded with premixed compositions of WC-Co, WC-Co+2.5wt%DD (or WC-Co+2.5DD), and WC-Co+5wt%DD (or WC-Co+5DD). Prior to loading the powder hopper, the powder mixtures were homogenously mixed on a ball mill without milling balls to avoid adjustment to the particle size distribution. Samples were printed as 15mm cross-sectional square patterns, onto a 3.4mm thick SS410 substrate according to the laser-power and scan speed machine settings shown in **Table 1**. Printing parameters were optimized over the course of 2-3 samples based on consistent visible deposition and bead formation characteristics on successive layers, and then 5 total samples were printed for each composition for testing and characterization. Layer thicknesses were calculated based on the overall sample height (as measured via optical microscopy) and divided by the 5-layers that were deposited, with the deposition head moving upwards at 200µm on each successive layer. The standard deviations are based on the variance in measurement of the overall deposit height when measured at different cross-section locations. Calculation of area percent porosity in the as-printed coatings was taken as the ratio of gas-pore area to overall coating area in two individual cross-sectional micrographs of polished specimens. The standard deviations are based on the variance in overall area fraction porosity across the total area of the images used in the porosity evaluation.

<u>Sample preparation for testing and analysis</u>: For microstructural characterization, as-printed samples were sectioned via water-jet cutter, mounted in phenolic resin and wet-ground on SiC paper from 60-2000 grit. Polishing was performed using an alumina-DI water solution from 1µ-0.05µ in particulate size. Before characterization, samples were ultrasonically cleaned with ethanol for 10 mins. Samples for hardness and reciprocating wear testing were left in the polished state. No etching was performed on any of the samples used for Scanning Electron

Microscopy (SEM) and Energy Dispersive Spectroscopy (EDS) (EDAX, Ametek, PA). Vickers indentation hardness testing (Phase II, Upper Saddle River, NJ) was done in accordance with ASTM standards on polished cross sections [31,32].

Tool geometry, preparation, and dry-turning test procedure: All tools used for machining were removed from the SS410 substrate via waterjet cutter and wet-ground to finish. The tools were chosen to be compared to the general-purpose VNMG 332 type cutting insert (Cobra Carbide, Riverside, CA, USA) which maintains a cutting-edge angle of 35° and is used in many general turning applications. To match the geometry, the printed tools were ground to a 35°±1 cutting edge with the top surface left in the as-processed condition. Chip breaking functionality was not incorporated in these tools to observe the chip formation during machining, and the tools engaged the workpiece transverse to the tip of the angled tool, without coolant. Two separate machining experiments (Tormach®, Waunakee, WI) were performed on standard barstock materials: one using aluminum alloy 6061-T6 at a conservative federate of 300SFM, and one using Ti6Al4V (TC4) alloy at a feedrate of 125SFM, to understand machining characteristics for a highly adhesive material in aluminum and a harder, more difficult-to-machine material in titanium. For both tests, machining was performed for the presented amount of time with the measured built up edge (BUE) measured from the outer edge of the BUE down the front (rake) surface of the tool. Measurements were taken after 1, 3, 5, and 10 minutes of machining, with a single tool used for each composition (8 total tools for aluminum and titanium machining). In both experiments, each tool was subjected to sequential passes (resulting in a minute's worth of machining) at a depth of cut of 0.127mm (0.005"). The aluminum barstock used for testing started as 1" in diameter and the titanium as 0.5" in diameter. To maintain the individual surface speeds, the following relation was used to adjust the spindle speed (RPM) to account for a slightly decreasing diameter from pass to pass:

$$RPM = \frac{V}{\pi D} \quad (1)$$

Where V is the cutting speed (mm/min), which was held constant, and D is the workpiece diameter (mm). After machining, no other surface treatment was done before performing EDS analysis on the tool surfaces to understand workpiece buildup and damage mechanisms using both tools. Machining tolerance was calculated as the difference between desired vs. actual final workpiece dimension as determined by the starting workpiece diameter, depth of cut, and number of successive passes.

3.0 Results

WC-Co + Diamond composites were successfully manufactured via directed-energy-deposition processing method. An initial set of process optimization was performed for the WC-Co base material, followed by process optimization of diamond dust incorporated WC-Co material. To understand the processability via additive manufacturing, microstructure, and resulting machining properties, extensive high magnification imaging as well as testing and analysis were performed and presented herein.

Processing, surface morphology, and porosity characteristics: Feedstock and choice of processing parameters played a large role in the resulting samples for each composition. All compositions were successfully printed separately via LENS™ technology (see **Fig. 2**). Both the WC-Co and diamond dust feedstock powders were highly granular in nature (**Figs.** 3**A1 & 3A2**), with the WC-Co powder size ranging from 75-100µm, and the diamond dust 25-75µm in overall size. The surfaces of the WC-Co particles were highly irregular, whereas, striations were observed on

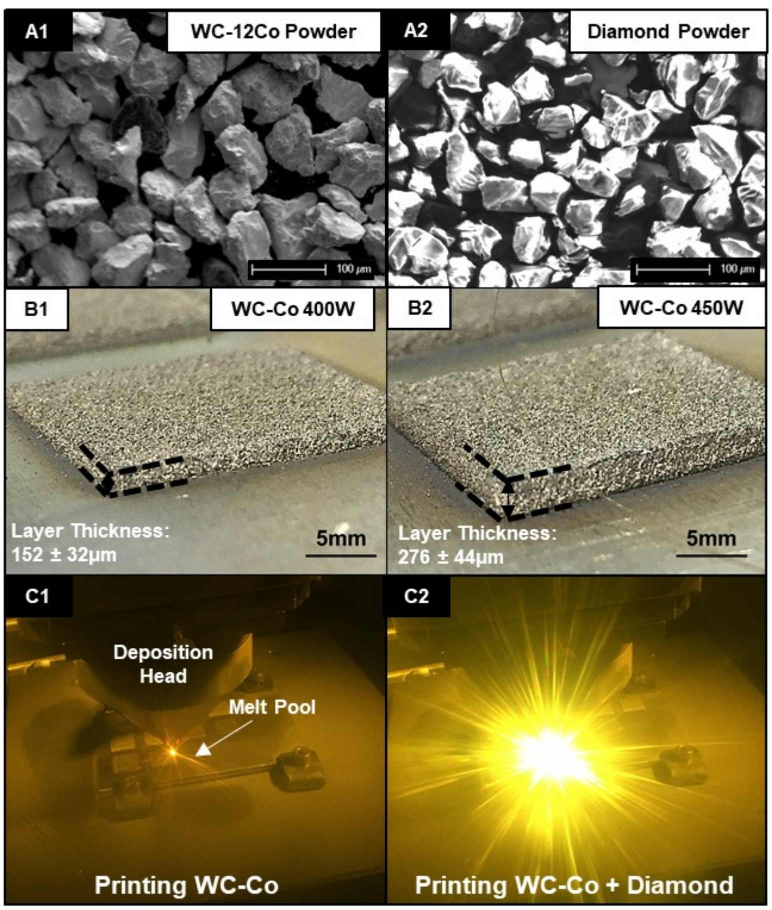

Figure 3: (A) Powder feedstock morphologies **(B)** Processing results of WC-Co at different parameters. **(C)** In-process view of printer and processed samples.

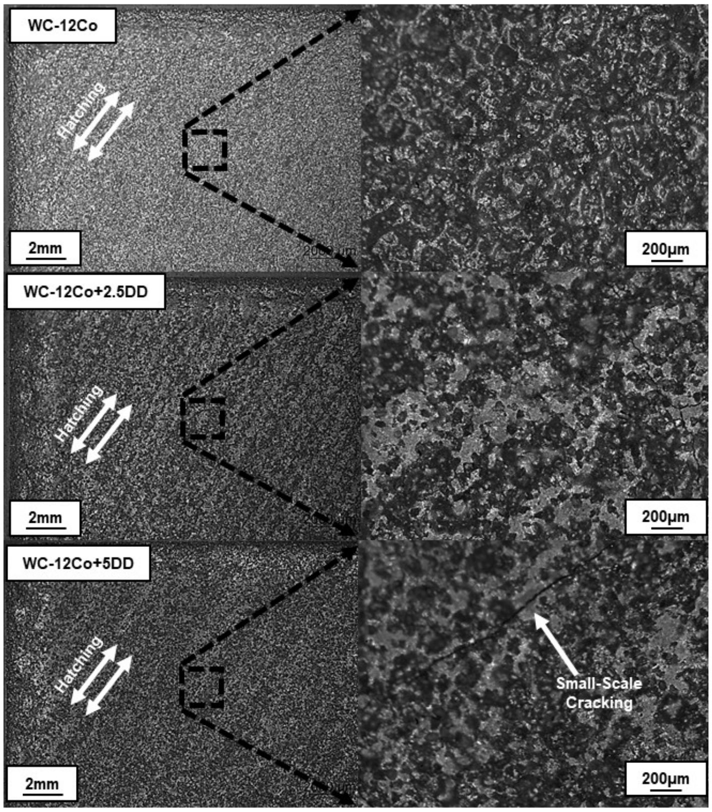

Figure 4: Top surface stereoscope images of each composition.

the surface of the diamond dust particles. All experimental samples were processed via LENS™ for five layers at 120° orientations to maintain consistent heating across the sample and decrease the chance for over-building and/or porosity in the as-printed samples. In addition, a constant hatch spacing of 0.5mm was utilized for all samples to maintain consistent track-to-track heating/melt-pool regimes. Prior to the deposition of the diamond dust containing compositions, the WC-Co base material system was optimized via several initial samples printed at parameters ranging from 400W-475W and scanning speeds of 5-6mm/s (see **Table 1)**. Initial samples at 400W resulted in low deposition height/layer thicknesses (152 ± 32µm) in comparison to the 450W and 475W (5-6mm/s) samples (286 ± 2 µm, 276 ± 44µm), see **Figure 3B1 & 3B2**. Higher than 475W processing power showed no increase in the visual deposited layer thickness, and multiple samples could be produced consistently, so these parameters were chosen for developing the base WC-Co tools, as well as the starting point for processing the diamond composition(s).

The addition of diamond dust to the WC-Co base material significantly affected processability and surface morphology. The view from outside the printer (behind laser shield) during the printing process for the WC-Co and diamond dust compositions is shown in **Fig. 3C1 & 3C2**. Processing of WC-Co resulted in a dull reflection of laser lighting from the melt pool, whereas, with the addition of diamond dust (both 2.5wt% as well as 5wt%), the melt pool become highly reflective, indicative of input power loss to the material due to lower overall absorptivity. Balling phenomena was apparent from using the processing parameters inherited from WC-Co for the WC-Co+5DD composition, so the scanning speed was increased from 5 to

7.5mm/s to reduce the tendency for overbuilding/balling to occur. From this, the resulting layer thicknesses for the 2.5DD and 5DD compositions were 158 ± 3µm and 132 ± 5µm, respectively, significantly lower compared to the WC-Co compositions. From the top surface micrographs of each composition in **Figure 4**, the hatching direction (120°) is readily visible, and each surface maintained a rough granular nature common for DED-based AM. The WC-Co and WC-Co+2.5DD compositions showed no indications of surface cracking, whereas, the WC-Co+5DD composition maintained several small-scale surface cracks ranging from 200-1000µm in length across the top surface.

Hardness, microstructure and phase analysis: **Figure 5** shows low magnification light micrographs of each composition's cross section. All interfaces, as well as bulk microstructures, were free from large-scale processing-parameter induced porosity (lack of fusion, keyholing) and cracking that is often associated with laser-based AM. Despite this, small spherical gas-pores were discovered within the coating (as outlined with green arrows). The area fraction of pores for the WC-Co composition was 0.39%±0.19% and increased to 1.18%±0.32% and 2.57%±0.15% for the 2.5DD and 5DD reinforced compositions, respectively. For the WC-Co and WC-Co+2.5DD compositions, pores were mostly found near the interface of the as-built structure, whereas for the WC-Co+5DD composition pores were found both within the bulk structure as well as near the interface. Further, each composition exhibited a transition region (**Fig. 5**) of approximately 200-250µm where the re-melted SS410 diffused into the cobalt and WC during printing. This resulted in a

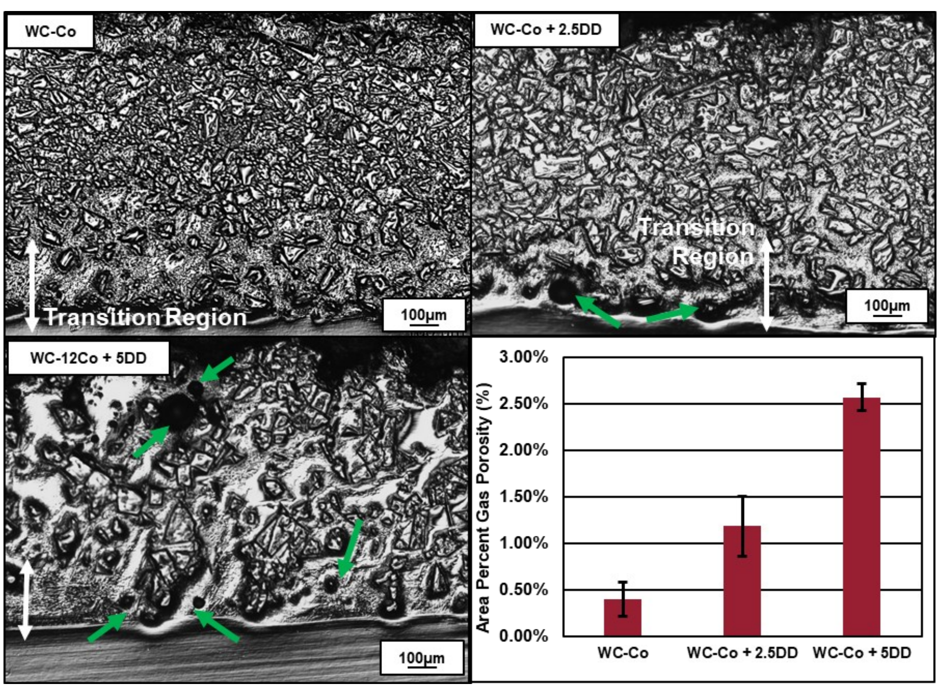

Figure 5: Cross section light microscope images of each composition and respective area fraction porosity.

region near the interface that maintained less distribution of WC-Co particles and more of a matrix, or binder, phase comprised of Co, Fe, and Cr, among others. EDS analysis (**Fig. 6**) highlights regions of Fe and Cr (from SS410) in the transition region, as well as the WC particles and W-rich dendritic phase with both primary and secondary arms that formed during the high-cooling rate processing. The transition region also exhibited a steady rise in hardness (**Fig.** 7) from the SS410 substrate ($200HV_{0.3/15}$-$500HV_{0.3/15}$) to the as-built material ($1100HV_{0.3/15}$-$1600HV_{0.3/15}$), with a relative spike at the top of the transition region for each composition. This transition leads to an ~5-6X increase in the hardness of the as-printed material relative to the substrate.

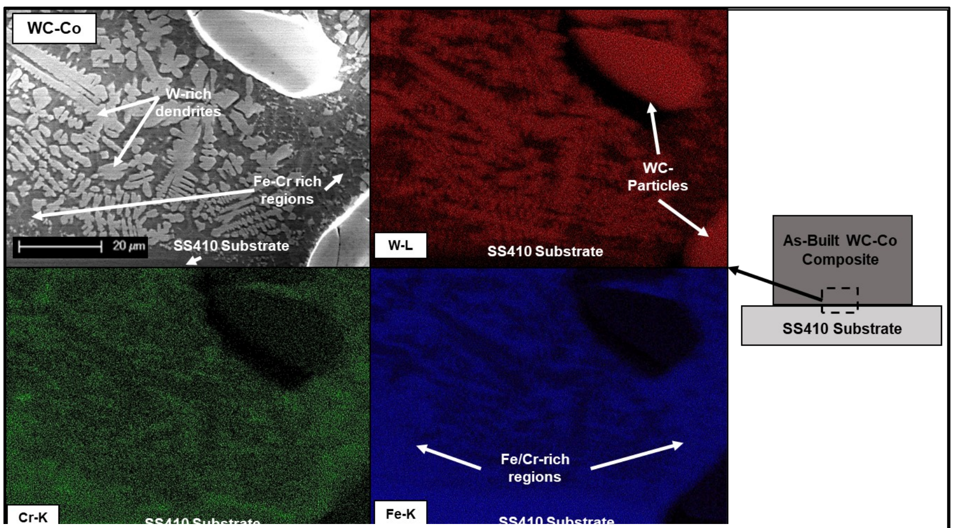

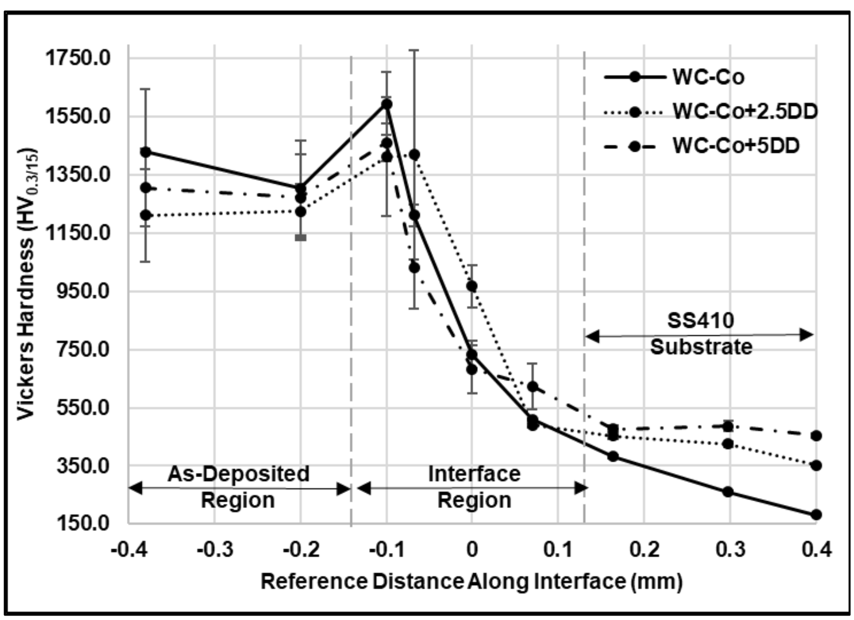

Figure 7: Cross section hardness profiles of each composition.

Deeper within the as-printed structures (**Fig. 8**), multiple reinforcing phases were formed during solidification and re-heating due to the layering scheme of laser-based AM. Both the WC-Co base composition and the diamond-containing compositions contained WC-particles as a primary phase in the range of 10-100µm, based on the locations of significant W-concentration (**Figs. 8A2 & 8B2**) as well as limited Co-concentration (**Figs. 8A3 & 8B3**). The resulting particle range in the as-printed structures indicates that *in situ* reactions have decreased some of the WC particle size down from the original 45-145μm starting size. Additionally, secondary phases include a Co-rich matrix (outlined as bright Co-regions with limited W-signature between large WC-particles in **Figs. 8A3 & 8B3**), as well as what is termed η-phase (Co_3W_3C) in the regions that are less Co-dominant but contain both W and Co-signatures, as has been shown in reference 22 [22]. Because of the small area fraction of regions without W-signature, it is assumed that within the small Co-rich matrix, there also resides some solutionized-W in the matrix.

From the backscattered electron images in **Figs. 9A1 & 9B1,** it is clear that the characteristic regions between the primary WC phase are different for the WC-Co and diamond containing compositions. Because different element density will provide distinctive contrast within a single image (brighter/more signal for higher density and vice versa), there are similar elemental characteristics (mainly tungsten) within regions between WC-particles in comparison to the WC-Co+2.5DD composition. In the diamond containing composition, the stark contrast between the matrix region and the WC-particles indicates that the diffusion of tungsten has been limited and that the matrix region has a significant amount of cobalt (and lesser η-phase) in comparison to the WC-Co composition. Further, the dendritic η-phase (outlined in white) that is shown forming in each composition near the interface (**Figs. 9A2 & 9B2**) maintains both primary and secondary growth for the WC-Co composition, whereas the morphology is more prismatic and scattered for the WC-Co+2.5DD composition.

Characteristic surface-level diamond dust particles within each diamond-containing composition are shown in **Figure 10**. In each diamond composition, the particles are well spread along the top surface with variable adhesion depth into the WC-Co matrix (as is shown in the SE image). It is clear from the BSE image that an elemental contrast is observed comparing the regions of the outlined particles to the overall matrix (tungsten-rich regions to carbon-rich regions). In addition, EDS analysis shows that the identified particles maintain limited Co or W signature, meaning that it is the diamond particles, as that is the only other feedstock material. Note that the dark region in the middle of the EDS image corresponds to an area where no signal could be identified owing to the variable surface height along the as-processed sample in relation to the detector.

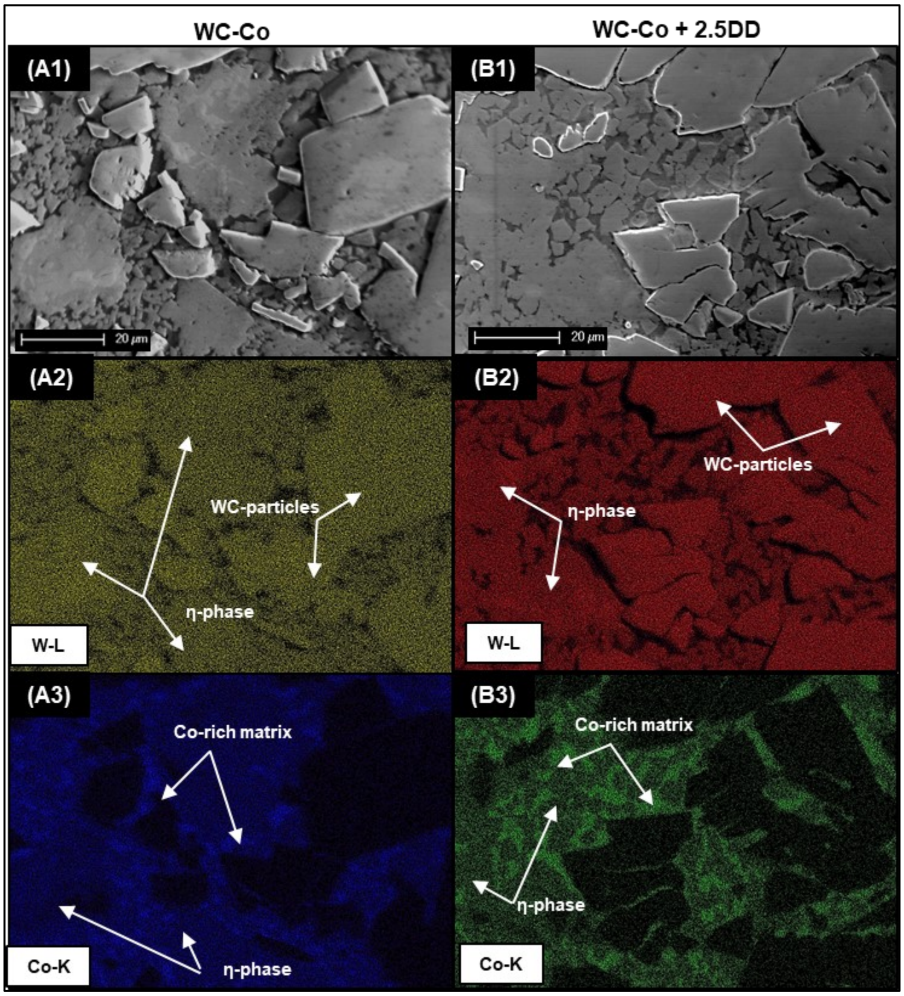

Figure 8: EDS analysis of high-magnification microstructures in areas of η-phase **(A)** WC-Co, and **(B)** WC-Co+2.5DD. Note that the η-phase is Co_3W_3C.

Figure 11 displays the XRD patterns of the feedstock powders as well as the as-processed top surface of each of the tested compositions. The diamond powder's main peak 43.9° (ICSD: 28857) is reflected in both the WC-Co-2.5DD and WC-Co-5DD compositions, with no significant difference in the peak intensities. The WC-Co powder exhibited two distinct WC (ICSD: 5212) peaks at 35.7° and 48.4°, which correspond to the two largest hexagonal-WC theoretical peaks. In addition, a small W_2C (39.8°) peak was observed, as well as two separate η-phase peaks (Co_3W_3C, ICSD: 166747). After processing the WC-Co powder via LENS™-based additive manufacturing, all peaks remained in addition to the emergence of a Co (FCC, ICSD: 44989) peak at 44.15°. With the introduction of 2.5wt%DD, the WC, W_2C, and η-phase peaks decrease substantially, the diamond peak emerges at 43.9°, and the cobalt peak at 44.15° increases as well as an additional peak emerges at 51°. The same overall phases were observed in the WC-Co+5DD composition as the WC-Co+2.5DD composition.

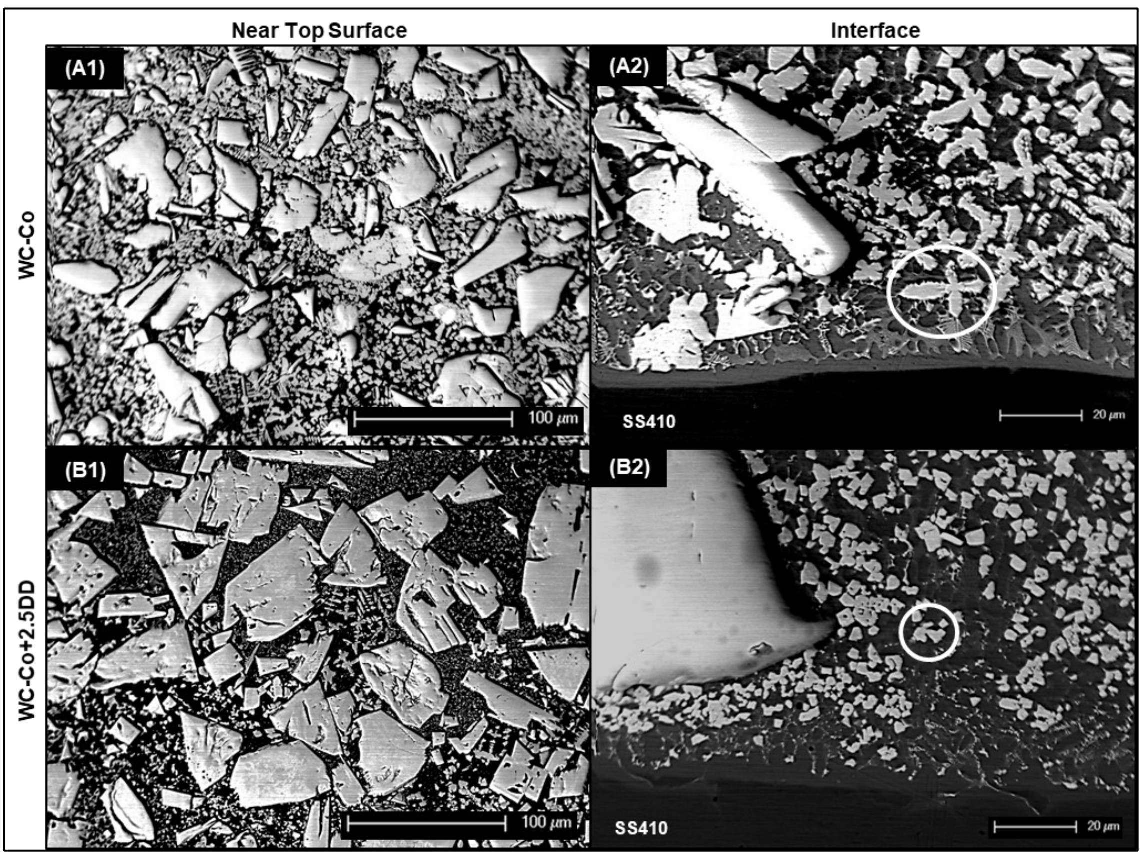

Figure 9: Backscattered-Electron (BSE) images of microstructures in **(A)** WC-Co, and **(B)** WC-Co+2.5DD.

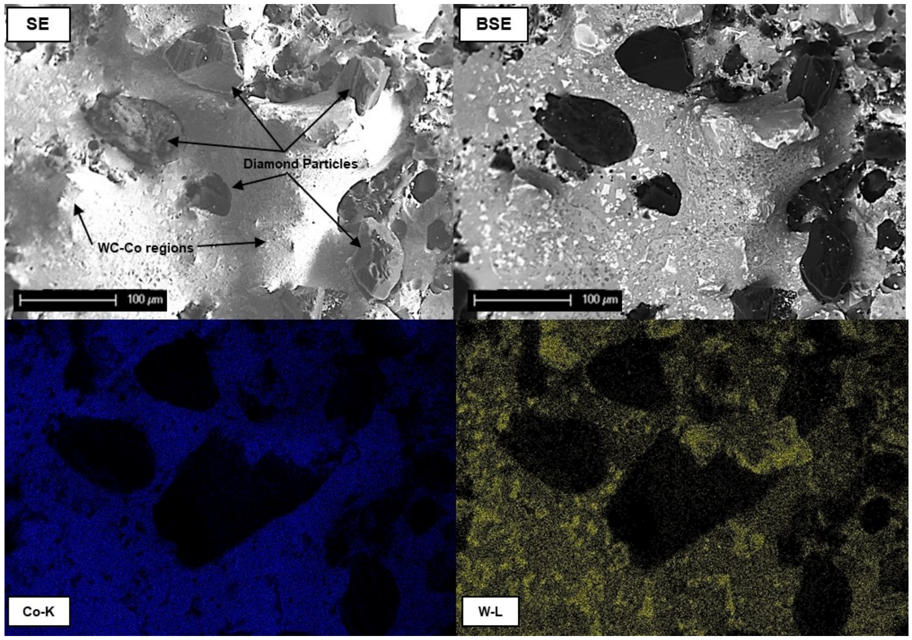

Figure 10: Secondary (SE), Backscattered-Electron (BSE) and EDS maps of top surface of WC-Co+5DD composition.

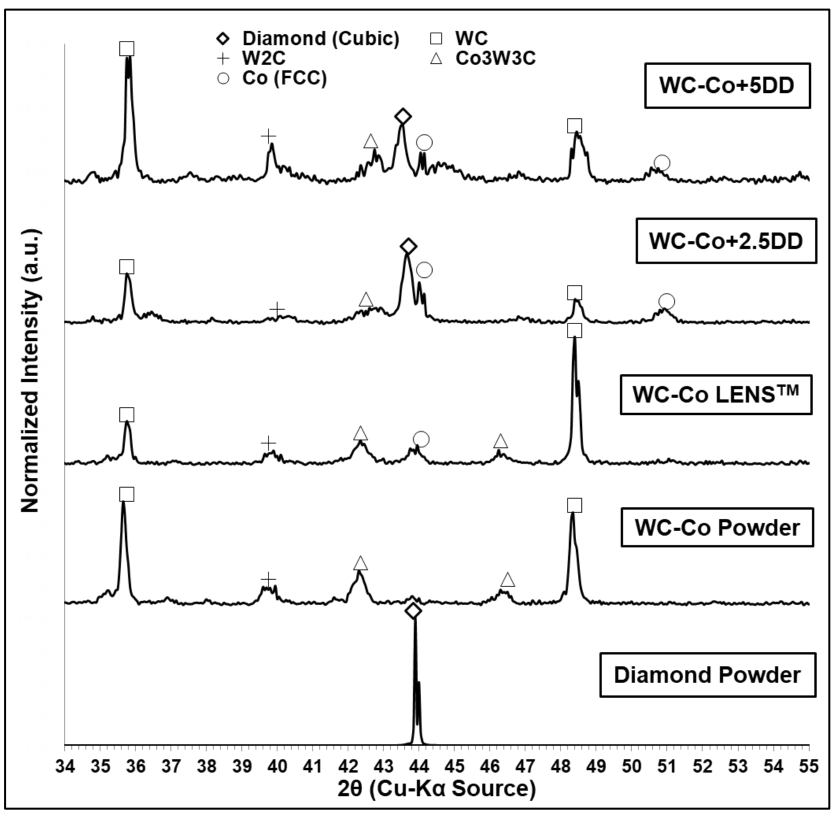

Figure 11: XRD analysis of feedstock powders and as-printed composites.

Machining performance of as-printed compositions: Machining parameters for each tool are outlined in **Fig. 12**, as well as the experimental outline and the setup. For all testing, tools remained intact with the SS304 silver soldered attachment with no loosening or fracture, and consistent chip formation was exhibited. Because Ti6Al4V is a much harder and more difficult-to-machine material, the chosen feedrate was significantly lower than that of Al6061-T6 (~0.03mm/min vs. 0.001mm/min), however, the same testing process was applied towards both materials in terms of tool setup, cutting, and built-up-edge size determination.

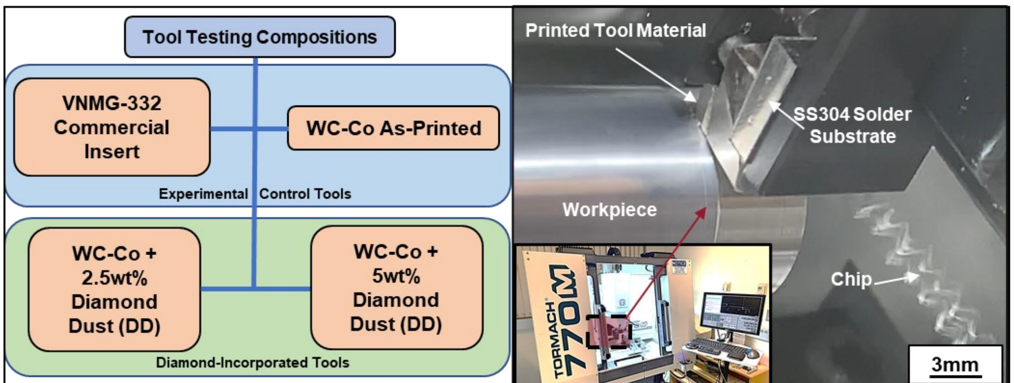

Material	Workpiece Diameter, D	Cutting Surface Speed, V	RPM Range	Depth of Cut	Traverse Speed (mm/min)	Feedrate (mm/rev)
Al6061-T6	1.0” (25.4mm)	300 ft/min (91 m/min)	1273-1338	0.005” (0.127mm)	40	0.030-0.031
Ti6Al4V	0.5” (12.7mm)	125 ft/min (91 m/min)	965-1061		20	0.020-0.019

Figure 12: (A) Tool testing experimental design. **(B)** Experimental tool testing setup using Tormach® 770M CNC Milling Machine. **(C)** Cutting parameters used for each tool on the corresponding workpiece.

Diamond incorporation to WC-Co played a significant role in reducing the BUE formation while machining the aluminum workpiece. **Figure 12** displays the leading edge of the tool with the machining direction towards the right of the image, and **Figure 13** outlines the measured BUE as well as the machining tolerance and wear mechanisms. Each tool exhibited increasing buildup of workpiece material during testing as shown in **Fig. 14A**. The commercial tool (which contains a chip breaker on the top surface), exhibited localized adhesion near the top surface that built up and continued building throughout testing to a steady value of 485±114µm after ten minutes. The as-printed WC-Co and WC-Co+2.5DD tools exhibited increasing BUE until 3 minutes of testing, where the values remained relatively constant and ended at 731±74µm and 395±91µm after ten minutes, respectively. The WC-Co+5DD tool experienced an increasing BUE from 1-5 minutes, however, the overall size decreased slightly during the final five-minute test to a final value of 312±32µm, ~35% lower than the commercial tool after ten minutes of testing. While the BUE was localized for the diamond-containing compositions, extensive

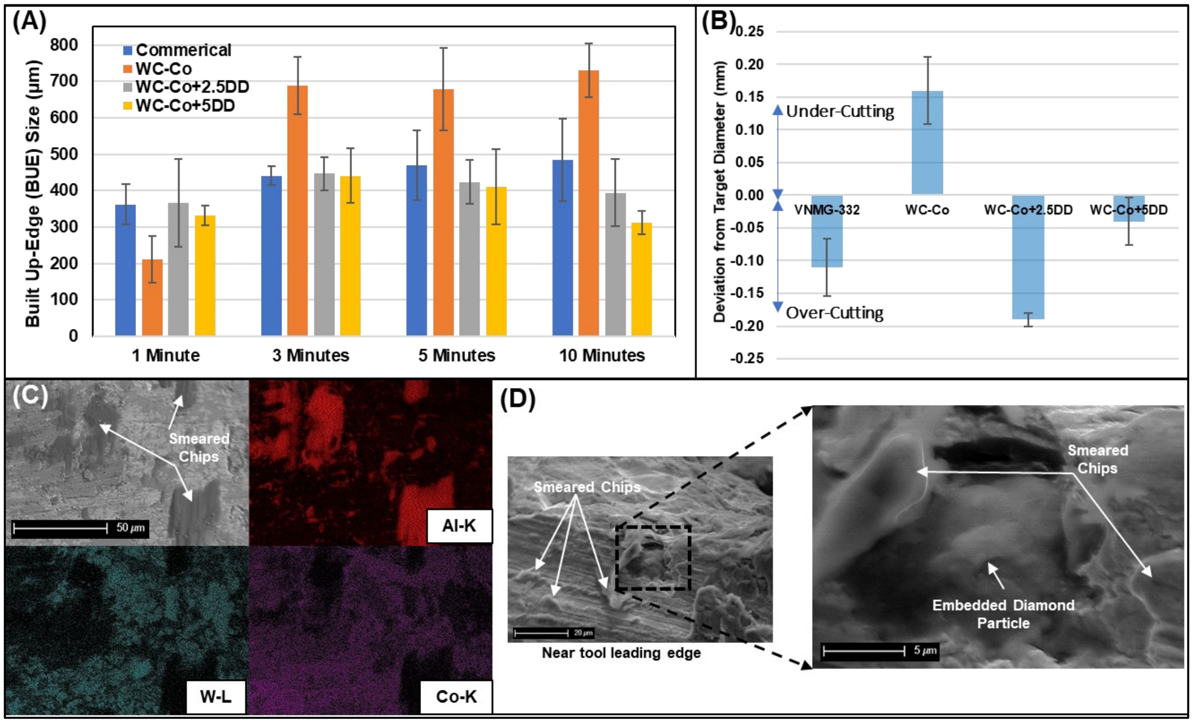

Figure 14: (A) Aluminum (Al-6061-T6) built-up-edge (BUE) values at different timepoints of machining for each composition. **(B)** Deviation from desired dimension for each composition. **(C)** High-magnification EDS of WC-Co LENS™ worn surface post-machining. **(D)** High-mag SEM image of WC-Co+5DD composition showing embedded diamond particle.

smearing was experienced by the WC-Co tool beginning at 5 minutes of testing and this continued till the end of testing resulting in a BUE value 50% higher than the commercial product, and 234% higher than the WC-Co+5DD composition. For the as-printed tools, slight smearing on the rake face was observed during testing which is common for single-point tested tools. In terms of machining dimensional tolerance (**Fig. 14B**), the WC-Co+5DD tool provided the closest-to-desired dimension, slightly over-cutting by 0.04mm (0.002") in comparison to the commercial tool that overcut the desired dimension by 0.11mm (0.004"). Further, **Fig. 14C** shows the worn surface of the WC-Co LENS™ composition where long (50-100µm) aluminum chips are highly smeared along the surface (as outlined by regions of high Al-concentration and limited W and Co signatures). In comparison to the WC-Co+5DD composition in **Fig. 14D**, the aluminum chips are much shorter (5-20µm), and are shown to smear along the surface of the WC/Co regions and are not adhered to the embedded diamond particles, indicating that the diamond resists adhesion to the surface of the tool during testing.

While machining titanium, diamond incorporation to WC-Co played a variable role in reducing the BUE formation from the workpiece. **Figure 15** displays the leading edge of the tool with the machining direction towards the right of the image, and **Figure 16** outlines the measured BUE as well as the machining tolerance and wear mechanisms. The commercial tool and WC-Co LENS™ exhibited increasing buildup of workpiece material during testing as shown in **Fig. 16A**. The commercial tool (also with a chip breaker), exhibited highly localized adhesion near the top surface that built up and reached relatively steady values until 418±72µm after ten minutes. The as-printed WC-Co+2.5DD and WC-Co+5DD tools reached relatively steady values after three minutes, ending at 150±17µm and 441±60µm after ten minutes, respectively. The WC-Co LENS™ experienced an increasing BUE from 1-5 minutes, however, the overall size decreased slightly during the final five-minute test to a final value of 649±17µm, ~55% higher than the commercial tool after ten minutes of testing. While the BUE was localized for the commercial tool, extensive chip adhesion and smearing was experienced by the WC-Co+5DD tool after 3 minutes of testing and this continued till the end of testing resulting in a BUE value 50% higher than the commercial product, and 234% higher than the WC-Co+2.5DD composition. For the WC-Co+2.5DD tool, slight adhesion on the rake face was observed which remained localized during testing, resulting in ~280% decrease in wear relative to the commercial tool. In terms of machining dimensional tolerance (**Fig. 16B**), the WC-Co+2.5DD tool provided the closest-to-desired dimension, slightly under-cutting by 0.01mm (0.001”) in comparison to the commercial tool that under-cut the desired dimension by 0.10mm (0.004”).

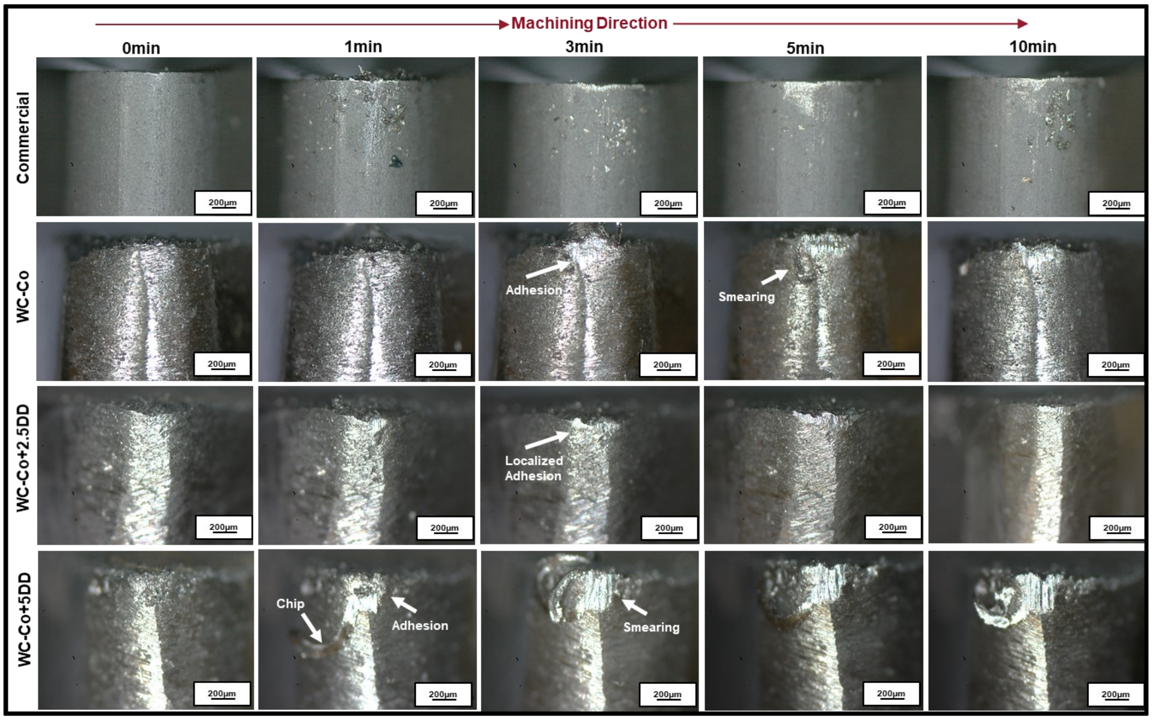

Figure 15: Built-up edge (BUE) optical micrographs of each tool after different time points of machining a Ti6Al4V (titanium alloy) workpiece.

Further, **Fig. 16C1** shows the worn surface of the WC-Co+2.5DD composition after ten minutes of machining, where diamond particles (as previously identified) are observed and still strongly adhered to the tool material, resisting abrasive wear and particle pullout. In addition, the horizontal striations from the grinding process are still observed on the tested cutting surface, indicating limited adhesion of the titanium workpiece to the tool. In heavy contrast, **Figure 16C2** shows the worn surface of the WC-Co+5DD composition after ten minutes of testing, where a spherical gas pore as well as diamond particle-pullout was observed, indicating a heavy amount of adhesive wear and high cutting forces from machining.

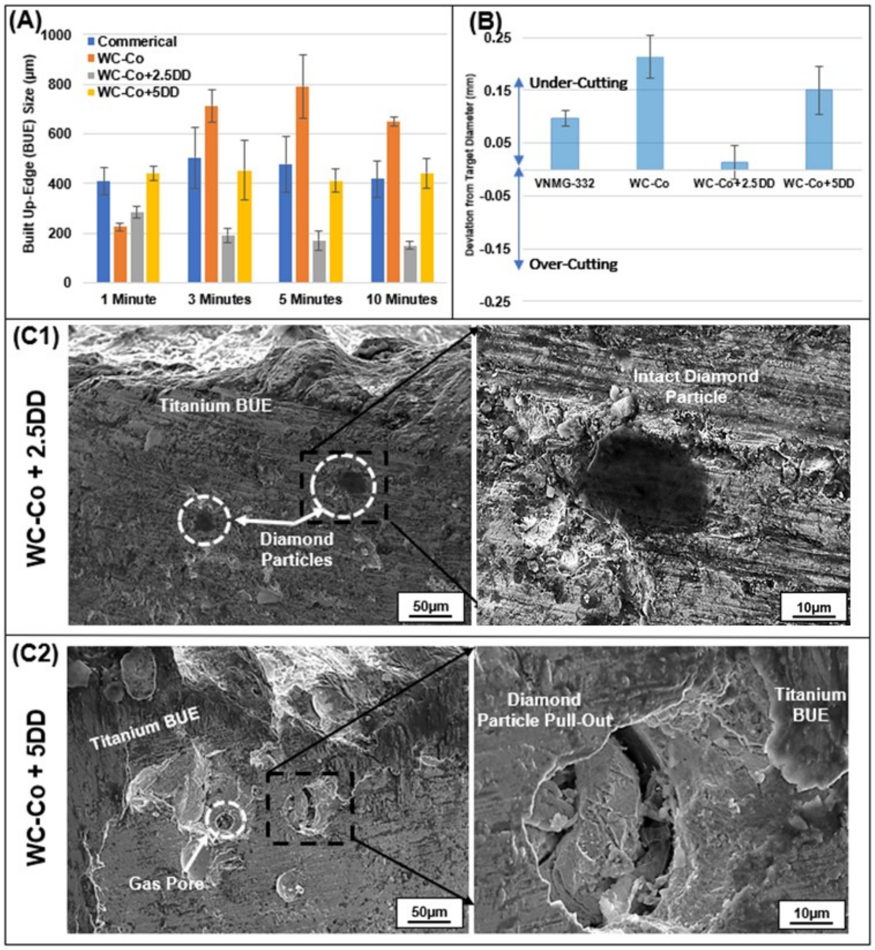

Figure 16: Titanium (Ti6Al4V) built-up edge (BUE) optical micrographs of each tool after different time points.

4.0 Discussion

Processing of WC-Co with Diamond Dust reinforcement: During laser-based AM of multi-material composites, there are several key processing variables as well as material properties that play a role in the melt pool, solidification, and final microstructure of the as-printed material[17]. In the case of directed energy deposition, with all other parameters and feedstock material properties held constant, the most influential parameters are the processing power and scanning speed, where higher power and lower speed results in a higher energy density and vice versa. In addition, key feedstock material properties that affect processing are the laser absorptivity and melting temperature of the printed material as they determine at what conditions the material will melt and solidify on the substrate. In the case of the composites processed in this study, the cobalt melts at a much lower temperature than WC/W_2C (1495C vs. 2870C), meaning that during processing the cobalt will melt and the WC particles will embed in the Co-matrix, resulting in several *in situ* phases and reactions. With all other parameters held constant (see **Table 1**), higher laser power and decreased scanning speed tended to increase the final sample height by 81% from 0.76 ± 0.16 to 1.38 ± 0.22mm. Because DED is a powder-flow AM method (as opposed to powder-bed), a finite amount of material is available to melt and solidify and the rest is cast to the side of the as-built structure through the continuous argon stream. Because of this, the increased build height is directly attributed to the increased amount of energy available for the cobalt within the feedstock to reach melting temperature, convert to liquid phase, and rapidly cool on the substrate. In comparison to other works, Balla et. al (2010) processed a similar composition at 350W and 450W with similar overall WC-particle distribution in the as-processed structures (compare with **Fig. 5**) and layer thickness[20], but higher porosity (2-3%) than the 0.4% than what was observed in this work, indicating the higher quality of the WC-Co processed herein. Although a different laser-based AM process, powder bed fusion (PBF) AM-based works have shown high porosity and cracking in similar WC-Co compositions [21,22,33]. In addition, the surface morphology of the WC-Co composition in the present study (**Fig. 4**) was comparable to that exhibited for a WC-25Co composition produced via PBF, with hatching lines visible and regions of both uniform and non-uniform melting [34]. Because DED-based processing contains a higher amount of unmelted particles on the surface (due to partial powder-flow hitting the top surface and partially-sintering), similar overall surface features to PBF-processed material indicates sufficient melting and high surface quality of the DED-processed material. This as-printed quality began to deteriorate with the addition of diamond dust because of the lower overall energy input achieved due to high-reflectivity (see **Figure 3C1 & 3C2**). This reduced energy input limited the available energy to the material to melt and re-solidify, reducing the overall build heights by 48-56% for the 2.5wt%DD and 5wt%DD additions. In addition, the reduced energy caused disturbances in the melt pool consistency relative to the parameters used in the WC-Co composition, as evidenced by the gas pores that infiltrated the microstructure both near the first few layers and throughout the overall structures. While these pores are common in AM-produced materials and can be tolerated if small (as in the case of the WC-Co+2.5DD material), the pores in the WC-Co+5DD (as large as 100µm in some areas), can greatly affect the properties of the as-printed structure. These pores, combined with the composite nature of the material with variable CTE and material properties throughout the hard and soft phases, can serve as sources of stress concentration that can cause cracking either during part operation or even due to the high thermal gradients and subsequent cooling rates inherent in laser-based AM. These factors are attributed to the small-scale surface cracking that was observed in the WC-Co+5DD composition (see **Figure 4**). Despite this characteristic, the machining performance was still improved over the WC-Co+2.5DD and commercial product for aluminum, but became a significant issue when machining the harder titanium material.

<u>Effects of diamond dust on processing and microstructures:</u> All compositions exhibited a 200-250μm transition region where the microstructures shift from being comprised of the SS410 base material and move into the WC-Co dendritic region. This transition region is depicted visually via EDS maps in **Fig. 6**, as well as through the hardness profile along the interface in **Fig. 7**. The gradual transition from the hardness of the SS410 to WC-Co, and EDS maps featuring significant Fe & Cr regions within the fusion zone indicate that on the first layer of processing, a significant amount of residual laser heating went into melting the top surface of the substrate. Despite the high melting temperature of WC (~2870°C), decarburization and solutioning of both W and C from WC particles into a Co-matrix has been exhibited, resulting in several precipitated phases within the microstructures [35]. Previous work has shown that the W-rich dendrites that form are of the W_2C metal carbide type, and that the matrix regions consist of an FCC Co-W solid solution (both phases present within the XRD analysis of **Fig. 11**) [36]. With the re-melting of the substrate on the first layer, the inter-dendritic regions likely receive excess Fe and Cr from the SS410 that contribute to the inter-dendritic matrix region(s). From a tool-processing standpoint, having this transition region is crucial to increased adhesion strength during cutting as well as increased heat transfer through the tool from the workpiece during operation, indicating the efficacy of this method to produce multi-layer structures capable of cutting standard engineering materials.

The bulk microstructures of the WC-Co cemented carbides were comprised of phases found during traditional processing as well as through other additive manufacturing methods. Li et al. (2018) previously described the solidification of WC-Co materials via PBF processing as the process of cooling from a liquid+metal carbide structure into a regime containing the η-phase, and then solidification of the Co-matrix [36]. While it was claimed that the η-phase is normally limited by its small formation temperature region of the phase diagram, reheating of previously deposited layers tended to form that phase in the microstructure [36]. Based on the high magnification images of **Figure 8** and XRD analysis in **Figure 11**, both the WC-Co and WC-Co+Diamond compositions were comprised of an FCC-Co matrix (with W in solution), WC/W_2C reinforcing phases as well as the η-phase in specific regions of the bulk structure. The presence of the η-phase is attributed to the reheating that occurs during laser-based AM that increases the cycles that reach the approximately 1500-1600C temperature region where the η-phase can form and remain in the microstructure. Despite the presence of the η-phase in the microstructures, comparing the relative amounts of the main η-phase peak at ~42.3° from the WC-Co composition to the WC-Co+2.5DD and WC-Co+5DD, shows a decrease with the addition of diamond (33% and 60% decrease in the peak intensities). This is also correlated with the BSE images of **Fig. 9**, where the presence of the η-phase (previously shown as similar complexion to the predominant WC phase and between the particles), tends to be of lesser amount than in the case of the WC-Co composition alone. Previous work based on calculated phase diagrams has shown that larger amounts of carbon within the mixture of a WC-Co-C system during solidification can decrease the relative amount of η-phase owing to the excess carbon present [37]. This shows that the addition of diamond, while also significantly affecting the processing characteristics, can also influence the phase fractions and microstructure of the cutting tools which can be beneficial in specific applications. While it has been shown in previous works that diamond can transform to graphite under high temperature laser processing, no evidence of graphitization occurred in the present work [25,26].

<u>Cutting performance of AM-produced tools</u>: Aluminum alloys are traditionally known for their ease in machinability, offering an adequate benchmark test for the efficacy of the additively manufactured WC-Co tools in the present study. For turning of aluminum alloys, tools that are highly adhesion resistant, sharp, and incorporate chip breaking features are desired to reduce the BUE effect, especially in the absence of coolant [38]. Because the geometry of the tools in this study was held constant and no chip breaking designed-mechanisms were incorporated, the decrease in BUE size is attributed directly to the composition of the tool. Diamond incorporation to WC-Co significantly decreased the BUE formation while machining the aluminum workpiece over time as shown in **Figs. 13 & 14**. While there was no designed chip-breaking mechanism, it has been shown that textured tool surfaces can provide beneficial machining characteristics such as decreased cutting forces, frictional forces, and surface temperature [39]. Because of this, the

rough surface from the powder-flow AM process likely contributed to the decrease in overall BUE and tight machining tolerance exhibited by the WC-Co+5DD composition, especially since aluminum is known as a highly adherent, "sticky" material to machine. Despite the presence of the η-phase within the microstructure, as well as internal porosity and residual stresses that occur during laser based AM[40], the WC-Co+5DD tool experienced the lowest overall BUE during the machining test at a final value of 312±32μm, ~35% lower than the commercial tool after ten minutes of testing, indicating that the tool is not only as good as the commercial product, but is improved in comparison to both the commercial and WC-Co/WC-Co+2.5DD compositions whose compositions exhibited smearing throughout testing, as well as continued buildup on the tool leading edges, respectively. It is important to note that the BUE values do not reflect what is commonly referred to as "tool wear", but rather the built up edge size relative to the top of the tool surface, where successive passes may result in continued buildup, or in the case of these tools, decreased or consistent buildup owing to the variabilities in the workpiece surface after engagement on successive passes. Further investigation (**Fig. 14C & 14D**) shows the decrease of adhesion on the worn surface of the WC-Co LENS™ composition from approx. 50-100μm aluminum chips are highly smeared along the surface, in comparison to the WC-Co+5DD composition where the aluminum chips are much shorter (5-20μm). The image of **Fig. 15D** clearly shows that the chips are limited in their ability to smear and adhere to the surface because of the strongly embedded diamond particles. This mechanism explains the extensive smearing experienced by the WC-Co tool beginning at 5 minutes of testing and this continued till the end of testing resulting in a BUE value 50% higher than the commercial product, and 234% higher than the WC-Co+5DD composition. Additionally, the WC-Co+5DD tool provided the closest-to-desired dimension, slightly over-cutting by 0.04mm (0.002") in comparison to the commercial tool that overcut the desired dimension by 0.11mm (0.004") and the WC-Co LENS™ tool that undercut by 0.16mm (~0.006"). While it is desired to have even lower than 0.025mm of tolerance in order to meet the needs of various parts with tight dimensional tolerance requirements that may require passes of less than 0.025mm, it is important to acknowledge that these tools have been hand-ground to size and automated tool-grinding processes can greatly increase this cutting tolerance. The tighter tolerance of the WC-Co+5DD composition is attributed to the smaller BUE which enables the tool to be sharper and provide a more consistent cut of the workpiece material. Further, although the reduced adherence of workpiece material characteristic of the WC-Co+5DD tool did not carry over into the machining of titanium, likely the lower cutting forces required to machine aluminum allowed the diamond particles to remain embedded in the WC-Co matrix and resist adhesion of the aluminum workpiece. The limited adhesion of aluminum to a diamond surface has been previously shown in the work of Rao and Shin (2001) as well as Gangopadhyay et al. (2010) who were studying face milling parameters on carbide and diamond coated inserts [41,42], and while in the present study coated inserts were not used, the same concept can be applied to the diamond particles that are reinforcing the WC-Co matrix material.

After demonstrating the efficacy of the diamond-reinforced tools to machine aluminum workpieces, it was integral to test the tools against a tougher to machine material such as titanium (**Figs. 15 & 16**). From a machining perspective, titanium is known for its relatively high hardness and low thermal conductivity, which typically requires significant coolant flow to reduce the tool tip temperatures and avoid a significant BUE or even coating failure. Research has shown that carbide tools with coatings such as TiAlN or PCD (plasma-coated-diamond) are recommended to operate at high cutting speeds and feeds [43], however adequate performance can be achieved with uncoated carbide tools. In the present study, diamond incorporation to WC-Co played a variable role in reducing the BUE formation from the workpiece. While the commercial and WC-Co LENS™ tools exhibited increasing buildup of workpiece material during testing as shown in **Fig. 15A** (resulting in as high as 55% greater BUE in comparison to the WC-Co+2.5DD composition), the as-printed WC-Co+2.5DD and WC-Co+5DD tools reached relatively steady values after three minutes, ending at 150±17μm and 441±60μm after ten minutes, indicative of higher performing tools that are resisting adhesion and BUE accumulation. **Fig. 16C1** shows the diamond particles (as previously identified) are strongly embedded within the WC-Co+2.5DD tool material, resisting abrasive wear and particle pullout, in comparison to the WC-Co+5DD composition which showed significant particle pullout (**Fig. 16C2**) and residual (spherical) gas pores. The worn surfaces indicate that the titanium, being a much harder and less conductive material, developed significantly higher cutting forces as well as heat that likely forced the diamond particles from strong adherence within the WC-Co matrix, causing the BUE to increase and deteriorate the tool surface for maintaining tight machining tolerances. These pores and particle pullout contributed to the decreased efficacy in reducing the BUE on the surface during machining, as well as a poor machining tolerance in comparison to the WC-Co+2.5DD tool and the commercial tool. As previously stated, while it is desired to have even lower than 0.025mm (0.001”) of tolerance in order to meet the needs of various parts with tight dimensional tolerance requirements that may require passes of less than 0.025mm (0.001”), it is important to acknowledge that these tools have been hand-ground to size and automated tool-grinding processes can greatly increase this cutting tolerance in addition to the measurement accuracy of 0.01mm of a digital caliper. Because the WC-Co+2.5DD tool machined to within 0.01mm, this indicates that the tool was as effective as could be measured via caliper and further detail would need to be measured with a different method. Despite the poor performance of the WC-Co+5DD tool in comparison to the WC-Co+2.5DD tool and commercial tool, it outperformed the WC-Co LENS™ tool both in overall BUE size after 10mins of machining and achievable tolerance, indicating that there was a moderate increase in machining performance despite the defects and pores in the microstructure. For the WC-Co+2.5DD tool, slight adhesion that was highly localized resulted in a ~280% decrease in wear relative to the commercial tool (36% of commercial tool’s value).

5. Future Directions

While this work demonstrates the ability to design tool materials and rapidly process multi-application carbide cutting tools via directed energy deposition, there are several key areas that could be explored from this work. Namely, while the as-printed materials were the same composition throughout the whole structure (as studied in-depth in this work), it can easily be envisioned that variable compositions along the height of the structures could provide higher-cost reinforcement materials such as diamond or other ceramics directly in the regions of cutting, leaving carbide and the cheaper substrate material below the cutting surface for backup after tool wear, reducing overall manufacturing and material costs. In addition, as the manufacturing industry continues to turn towards additive-based processes for producing end-use components, this work demonstrates that parts and tools can be manufactured via the same process, i.e. directed energy deposition, therefore decreasing the supply chain relative to the multi-process procedures for producing tooling and parts traditionally. **Fig. 17A** displays one of the studied

AM-tools turning a DED-produced titanium cylinder in the same experimental setup that was used for the present work. As was shown in the case of the Ti6Al4V barstock, the WC-Co+2.5DD composition demonstrated improved performance over the commercially-available insert of similar composition. This capability demonstrates that tools and parts can be manufactured in parallel and different tool materials, geometries, and coatings can be catered to machine the specific feedstocks that are designed for application-specific needs. Additionally,

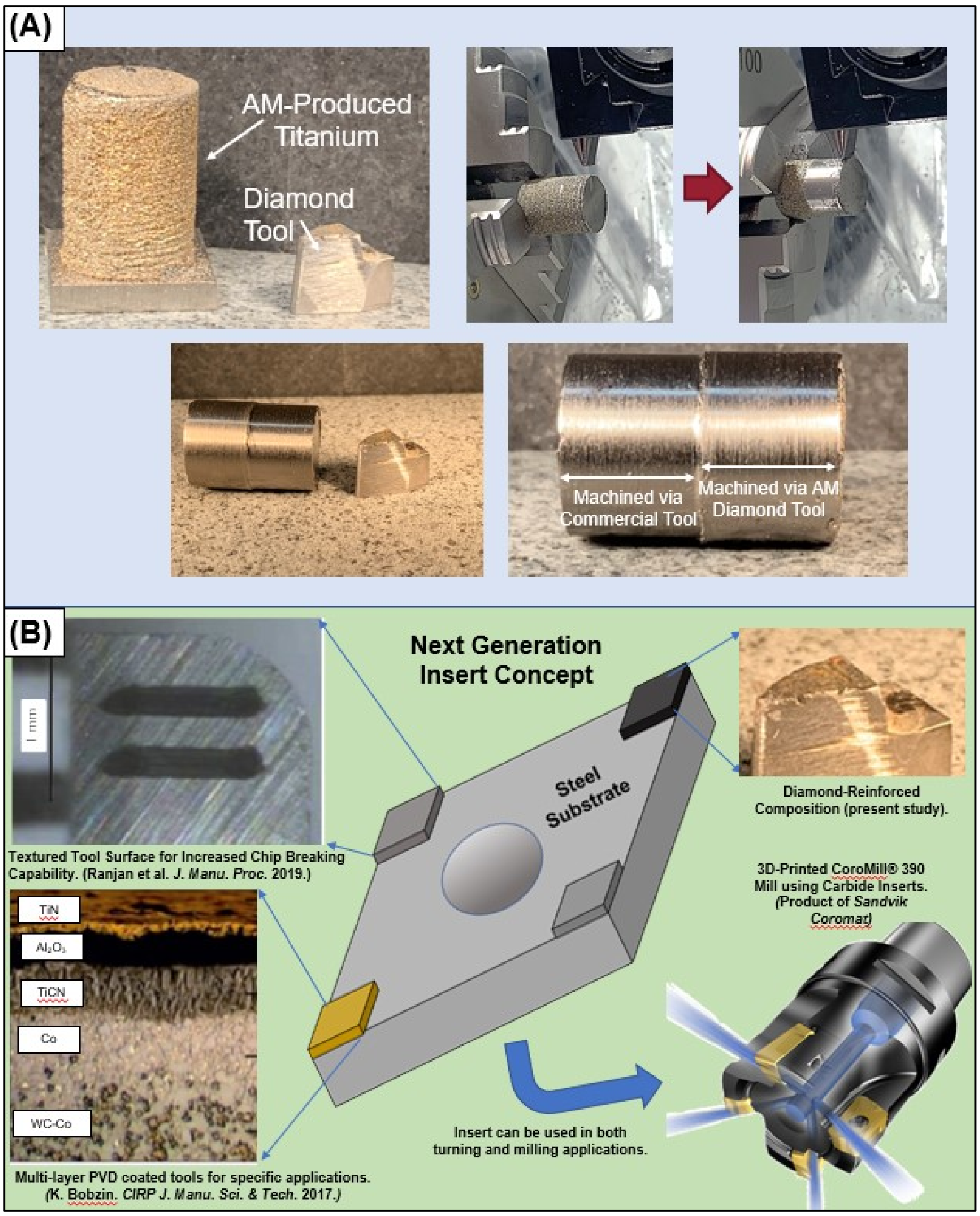

Figure 17: Next generation insert concepts implicated with the present study. **(A)** Example of AM-produced titanium being machined by a commercial tool as well as the WC-Co+2.5DD tool examined in the presented study. **(B)** Potential insert cutting surfaces for different cutting applications/workpieces.

Fig.17B highlights the potential for this cutting tool processing method to incorporate different tool concepts within the same tool by variable composition deposition. More specifically, emerging coating schemes using different ceramic layers can be envisioned (bottom left)[44], as well as textured surfaces that can aid in BUE formation with different materials (top left)[39]. These concepts, coupled with the work shown in the present study (diamond-reinforcement) can also be incorporated into milling cutters that utilize indexable inserts, meaning that not only turning but also milling operations can be accomplished with these inserts.

6. Conclusions

Diamond reinforced carbide coatings were manufactured via DED-based AM technology in order to demonstrate the ability to process next generation of cutting tools. Diamond incorporation had a remarkable effect on the processing, microstructure, and machining performance of the WC-Co base material in comparison to a commercial carbide cutting tools of similar composition to the WC-Co AM-produced material. Despite the presence of the η-phase in the microstructures of the as-processed composites, which is known to be detrimental to machining performance, diamond reinforcement contributed to a decrease in the relative η-phase amount compared to the as-processed WC-Co, resulting in the lowest overall built up edge during machining of both aluminum and titanium, in addition to high adhesion resistance along the tool surfaces. The WC-Co+5DD composition exhibited a 35% lower BUE than the commercial tool after ten minutes of machining aluminum, and the WC-Co+2.5DD tool exhibited 64% decrease in BUE overall size compared to the commercial tool while machining titanium, indicating that these tools outperform what is currently available on the market due to innovative compositional design and processing via AM. Our work demonstrates the ability to exploit laser-based AM to create cutting tools that are multifunctional and meet next-generation of manufacturing demands.

7. Acknowledgements

Authors would like to acknowledge financial support from the National Science Foundation under the grant number NSF-CMMI 1934230 (PI - Bandyopadhyay), and the

National Institute of Arthritis and Musculoskeletal and Skin Diseases of the National Institutes of Health under Award Number R01 AR067306-01A1. The content is solely the responsibility of the authors and does not necessarily represent the official views of the National Institutes of Health. Authors also acknowledge assistance with XRD from Dr. Thomas Williams from the University of Idaho.

Data availability

The data that support the findings of this study are available from the corresponding author on reasonable request.

Declaration of Competing Interest

All authors declare that they have no competing interests for this publication.

8. References

[1] Machining Market to Reach $414.17 Billion by 2022, Says Beroe Inc, CISION PR Newswire. (2019). https://www.prnewswire.com/news-releases/machining-market-to-reach-414-17-billion-by-2022--says-beroe-inc-300939464.html.

[2] E. MacDonald, R. Wicker, Multiprocess 3D printing for increasing component functionality, Science (80-.). (2016). doi:10.1126/science.aaf2093.

[3] D. Axinte, J. Billingham, A. Bilbao Guillerna, New models for energy beam machining enable accurate generation of free forms, Sci. Adv. 3 (2017) e1701201. doi:10.1126/sciadv.1701201.

[4] A. Bandyopadhyay, B. Heer, Additive manufacturing of multi-material structures, Mater. Sci. Eng. R Reports. 129 (2018) 1–16. doi:10.1016/j.mser.2018.04.001.

[5] E. O. Bennett, Water based cutting fluids and human health, Tribol. Int. 16 (1983) 133–136. doi:10.1016/0301-679X(83)90055-5.

[6] G. S. Goindi, P. Sarkar, Dry machining: A step towards sustainable machining – Challenges and future directions, J. Clean. Prod. (2017). doi:10.1016/j.jclepro.2017.07.235.

[7] M. Gomez, J. Heigel, T. Schmitz, Force modeling for hybrid manufacturing, Procedia

Manuf. 26 (2018) 790–797. doi:10.1016/j.promfg.2018.07.096.

[8] K. Cheng, ed., Machining Dynamics, Springer London, London, 2009. doi:10.1007/978-1-84628-368-0.

[9] Metal AM Magazine, Kennametal launches Additive Manufacturing business unit, Inovar Commun. Ltd. (2019). https://www.metal-am.com/kennametal-launches-additive-manufacturing-business-unit/.

[10] L. D. Bobbio, R.A. Otis, J.P. Borgonia, R.P. Dillon, A.A. Shapiro, Z.K. Liu, A.M. Beese, Additive manufacturing of a functionally graded material from Ti-6Al-4V to Invar: Experimental characterization and thermodynamic calculations, Acta Mater. 127 (2017) 133–142. doi:10.1016/j.actamat.2016.12.070.

[11] B. Onuike, B. Heer, A. Bandyopadhyay, Additive manufacturing of Inconel 718—Copper alloy bimetallic structure using laser engineered net shaping (LENS^{TM}), Addit. Manuf. 21 (2018) 133–140. doi:10.1016/j.addma.2018.02.007.

[12] B. E. Carroll, R.A. Otis, J.P. Borgonia, J.O. Suh, R.P. Dillon, A.A. Shapiro, D.C. Hofmann, Z.K. Liu, A.M. Beese, Functionally graded material of 304L stainless steel and inconel 625 fabricated by directed energy deposition: Characterization and thermodynamic modeling, Acta Mater. 108 (2016) 46–54. doi:10.1016/j.actamat.2016.02.019.

[13] D. C. Hofmann, J. Kolodziejska, S. Roberts, R. Otis, R.P. Dillon, J.-O. Suh, Z.-K. Liu, J.-P. Borgonia, Compositionally graded metals: A new frontier of additive manufacturing, J. Mater. Res. 29 (2014) 1899–1910. doi:10.1557/jmr.2014.208.

[14] D. C. Hofmann, S. Roberts, R. Otis, J. Kolodziejska, R.P. Dillon, J.O. Suh, A.A. Shapiro, Z.K. Liu, J.P. Borgonia, Developing gradient metal alloys through radial deposition additive manufacturing, Sci. Rep. 4 (2014). doi:10.1038/srep05357.

[15] T. Shin, Y.-S. Kim, J. Kim, K.-Y. Lee, S.-J. Lee, D. Sun, Y.-W. Lim, D. Lim, Applicability evaluation of direct metal tooling-based additive manufacturing for reducing ceramic liner fracture in total hip arthroplasty, Surf. Coatings Technol. 347 (2018) 313–319. doi:10.1016/j.surfcoat.2018.04.030.

[16] R. Leal, F. M. Barreiros, L. Alves, F. Romeiro, J. C. Vasco, M. Santos, C. Marto, Additive manufacturing tooling for the automotive industry, Int. J. Adv. Manuf. Technol. 92 (2017) 1671–1676. doi:10.1007/s00170-017-0239-8.

[17] K. D. Traxel, A. Bandyopadhyay, Reactive-deposition-based additive manufacturing of Ti-Zr-BN composites, Addit. Manuf. 24 (2018). doi:10.1016/j.addma.2018.10.005.

[18] S. Pouzet, P. Peyre, C. Gorny, O. Castelnau, T. Baudin, F. Brisset, C. Colin, P. Gadaud, Additive layer manufacturing of titanium matrix composites using the direct metal deposition laser process, Mater. Sci. Eng. A. 677 (2016) 171–181. doi:10.1016/j.msea.2016.09.002.

[19] K. D. Traxel, A. Bandyopadhyay, First Demonstration of Additive Manufacturing of Cutting Tools using Directed Energy Deposition System: Stellite^{TM}-Based Cutting Tools, Addit. Manuf. 25 (2019) 460–468. doi:10.1016/j.addma.2018.11.019.

[20] V. K. Balla, S. Bose, A. Bandyopadhyay, Microstructure and wear properties of laser deposited WC–12%Co composites, Mater. Sci. Eng. A. 527 (2010) 6677–6682. doi:10.1016/j.msea.2010.07.006.

[21] R. S. Khmyrov, V. A. Safronov, A. V. Gusarov, Obtaining Crack-free WC-Co Alloys by Selective Laser Melting, Phys. Procedia. 83 (2016) 874–881. doi:10.1016/j.phpro.2016.08.091.

[22] S. Kumar, A. Czekanski, Optimization of parameters for SLS of WC-Co, Rapid Prototyp. J. 23 (2017) 1202–1211. doi:10.1108/RPJ-10-2016-0168.

[23] B. L. Boyce, B. C. Salzbrenner, J. M. Rodelas, L. P. Swiler, J. D. Madison, B. H. Jared, Y.-L. Shen, Extreme-Value Statistics Reveal Rare Failure-Critical Defects in Additive Manufacturing, Adv. Eng. Mater. 19 (2017) 1700102. doi:10.1002/adem.201700102.

[24] O. Holzmond, X. Li, In situ real time defect detection of 3D printed parts, Addit. Manuf. 17 (2017) 135–142. doi:10.1016/j.addma.2017.08.003.

[25] X. Fang, Z. Yang, S. Tan, L. Duan, Feasibility Study of Selective Laser Melting for Metal Matrix Diamond Tools, Crystals. 10 (2020) 596. doi:10.3390/cryst10070596.

[26] A. B. Spierings, C. Leinenbach, C. Kenel, K. Wegener, Processing of metal-diamond-composites using selective laser melting, Rapid Prototyp. J. 21 (2015) 130–136. doi:10.1108/RPJ-11-2014-0156.

[27] H. M. Yehia, O. El-Kady, A. Abu-Oqail, Effect of diamond additions on the microstructure, physical and mechanical properties of WC- TiC- Co/Ni Nano-composite, Int. J. Refract. Met. Hard Mater. 71 (2018) 198–205. doi:10.1016/j.ijrmhm.2017.11.018.

[28] G. S. Bobrovinitchii, A. L. D. Skury, M. Filgueira, S. N. Monteiro, R.C. Tardim, Study on

WC-Co-Diamond-Based Composites Used in Cutters of Drill Bits, Mater. Sci. Forum. 660–661 (2010) 489–494. doi:10.4028/www.scientific.net/MSF.660-661.489.

[29] H. Sahasrabudhe, A. Bandyopadhyay, Additive Manufacturing of Reactive In Situ Zr Based Ultra-High Temperature Ceramic Composites, JOM. 68 (2016) 822–830. doi:10.1007/s11837-015-1777-x.

[30] A. Uriondo, M. Esperon-Miguez, S. Perinpanayagam, The present and future of additive manufacturing in the aerospace sector: A review of important aspects, Proc. Inst. Mech. Eng. Part G J. Aerosp. Eng. 229 (2015) 2132–2147. doi:10.1177/0954410014568797.

[31] ASTM Standard E384-16, Test Method for Microindentation Hardness of Materials, ASTM International, West Conshohocken, PA, PA, 2016. doi:10.1520/E0384-16.

[32] ASTM Standard C1327, W. Conshohocken, ASTM Standard C1327, Test Method for Vickers Indentation Hardness of Advanced Ceramics, ASTM International, West Conshohocken, PA, PA, 2015. doi:10.1520/C1327-08.2.

[33] E. Uhlmann, A. Bergmann, W. Gridin, Investigation on Additive Manufacturing of Tungsten Carbide-cobalt by Selective Laser Melting, Procedia CIRP. 35 (2015) 8–15. doi:10.1016/j.procir.2015.08.060.

[34] R. S. Khmyrov, A. P. Shevchukov, A. V. Gusarov, T. V. Tarasova, Phase composition and microstructure of WC–Co alloys obtained by selective laser melting, Mech. Ind. 18 (2017) 714. doi:10.1051/meca/2017059.

[35] J. Yuan, Q. Zhan, J. Huang, S. Ding, H. Li, Decarburization mechanisms of WC–Co during thermal spraying: Insights from controlled carbon loss and microstructure characterization, Mater. Chem. Phys. 142 (2013) 165–171. doi:10.1016/j.matchemphys.2013.06.052.

[36] C.-W. Li, K.-C. Chang, A.-C. Yeh, J.-W. Yeh, S.-J. Lin, Microstructure characterization of cemented carbide fabricated by selective laser melting process, Int. J. Refract. Met. Hard Mater. 75 (2018) 225–233. doi:10.1016/j.ijrmhm.2018.05.001.

[37] L. Åkesson, An Experimental and Thermodynamic Study of the Co-W-C system in the temperature range 1473-1698K, Royal Institue of Technology, Stockholm Sweden, 1982.

[38] T. R. Soren, R. Kumar, I. Panigrahi, A. K. Sahoo, A. Panda, R. K. Das, Machinability behavior of aluminium alloys: A brief study, in: Mater. Today Proc., 2019. doi:10.1016/j.matpr.2019.07.502.

[39] P. Ranjan, S.S. Hiremath, Role of textured tool in improving machining performance: A review, J. Manuf. Process. 43 (2019) 47–73. doi:10.1016/j.jmapro.2019.04.011.

[40] A. Bandyopadhyay, K.D. Traxel, Invited review article: Metal-additive manufacturing—Modeling strategies for application-optimized designs, Addit. Manuf. 22 (2018) 758–774. doi:10.1016/j.addma.2018.06.024.

[41] B. Rao, Y.C. Shin, Analysis on high-speed face-milling of 7075-T6 aluminum using carbide and diamond cutters, Int. J. Mach. Tools Manuf. (2001). doi:10.1016/S0890-6955(01)00033-5.

[42] S. Gangopadhyay, R. Acharya, A.K. Chattopadhyay, V.G. Sargade, EFFECT OF CUTTING SPEED AND SURFACE CHEMISTRY OF CUTTING TOOLS ON THE FORMATION OF BUL OR BUE AND SURFACE QUALITY OF THE GENERATED SURFACE IN DRY TURNING OF AA6005 ALUMINIUM ALLOY, Mach. Sci. Technol. 14 (2010) 208–223. doi:10.1080/10910344.2010.500961.

[43] R. M'Saoubi, D. Axinte, S.L. Soo, C. Nobel, H. Attia, G. Kappmeyer, S. Engin, W.-M. Sim, High performance cutting of advanced aerospace alloys and composite materials, CIRP Ann. 64 (2015) 557–580. doi:10.1016/j.cirp.2015.05.002.

[44] K. Bobzin, High-performance coatings for cutting tools, CIRP J. Manuf. Sci. Technol. (2017). doi:10.1016/j.cirpj.2016.11.004.